

# Fokker-Planck equation driven by asymmetric Lévy motion

Xiao Wang<sup>1</sup>, Wenpeng Shang<sup>1</sup>, Xiaofan Li<sup>2\*</sup>, Jinqiao Duan<sup>2</sup>, Yanghong Huang<sup>3</sup>

<sup>1</sup> *School of Mathematics and Statistics, Henan University*

*Kaifeng 475001, China*

*email xwang@vip.henu.edu.cn*

<sup>2</sup> *Department of Applied Mathematics, Illinois Institute of Technology*

*Chicago, IL 60616, USA*

*email lix@iit.edu(X. Li), duan@iit.edu(J. Duan)*

<sup>3</sup> *Department of Applied Mathematics, University*

*School of Mathematics, The University of Manchester, Manchester, M13 9PL, UK*

*email yanghong.huang@manchester.ac.uk*

March 5, 2018

## Abstract

Non-Gaussian Lévy noises are present in many models for understanding underlining principles of physics, finance, biology and more. In this work, we consider the Fokker-Planck equation(FPE) due to one-dimensional asymmetric Lévy motion, which is a nonlocal partial differential equation. We present an accurate numerical quadrature for the singular integrals in the nonlocal FPE and develop a fast summation method to reduce the order of the complexity from  $O(J^2)$  to  $O(J \log J)$  in one time-step, where  $J$  is the number of unknowns. We also provide conditions under which the numerical schemes satisfy maximum principle. Our numerical method is validated by comparing with exact solutions for special cases. We also discuss the properties of the probability density functions and the effects of various factors on the solutions, including the stability index, the skewness parameter, the drift term, the Gaussian and non-Gaussian noises and the domain size.

*Key words:* Non-Gaussian noises, Fokker-Planck equations, asymmetric  $\alpha$ -stable Lévy motion, nonlocal partial differential equation, fast algorithm

## 1 Introduction

The Fokker-Planck equation (FPE) was first used to describe the Brownian motion of particles, which gives the time evolution of the probability density function for the systems [12, 26]. For stochastic differential equations (SDEs) driven by Brownian motion, the corresponding FPE is a second-order parabolic partial differential equation. For some special cases, the analytic solutions can be founded but in general people seek numerical solutions with well-developed numerical methods for such differential equations. However, noisy fluctuations are usually non-Gaussian in nature, and the investigation of the FPE induced by non-Gaussian noises is still in its infancy. Non-Gaussian noises are widely found to describe the phenomenon in physics, biology, economics among other fields [4, 19, 38]. In this work, we consider FPEs derived from stable Lévy motion because of its properties of 'heavy tail' and central limit theorem.

---

\*Corresponding author. E-mail: lix@iit.edu

A Lévy motion is a stochastic process which has independent and stationary increments, stochastically continuous sample paths. It is completely determined by the Lévy-Khintchine formula, i.e. a Lévy motion is characterized by the generating triplet  $(b, A, \nu)$ ,  $b$  is a drift vector,  $A$  is a diffusion matrix and  $\nu$  is an Lévy measure satisfying  $\int_{\mathbb{R}^n \setminus \{0\}} (|y|^2 \wedge 1) \nu(dy) < \infty$ .

In this paper, we mainly consider FPEs corresponding to scalar SDEs with stable Lévy motion whose distribution  $S_\alpha(\tau, \beta, \mu)$  is determined by four parameters: the index of stability  $\alpha$  ( $0 < \alpha \leq 2$ ), the scaling parameter  $\tau$  ( $\tau \geq 0$ ), the skewness parameter ( $-1 \leq \beta \leq 1$ ) and the shift parameter  $\mu$ . The Lévy-Khintchine formula for the stable Lévy motion is [16, 29]

$$\mathbb{E}(e^{i\lambda L_t}) = \begin{cases} \exp\{-\tau^\alpha |\lambda|^{\alpha t} (1 - i\beta \operatorname{sgn} \lambda \tan \frac{\pi\alpha}{2}) + i\mu\lambda t\}, & \text{for } \alpha \neq 1, \\ \exp\{-\tau |\lambda| t (1 + i\beta \frac{2}{\pi} \operatorname{sgn} \lambda \log |\lambda|) + i\mu\lambda t\}, & \text{for } \alpha = 1. \end{cases} \quad (1.1)$$

The  $\alpha$ -stable random variable is strictly stable for  $\mu = 0$  and  $\alpha \neq 1$ , but when  $\alpha = 1$ , it is strictly stable if and only if the process is symmetric ( $\beta = 0$ ). We take  $\sigma = 1$  and  $\mu = 0$  for consideration.

Recently, numerous research focus on the symmetric stable Lévy motion, corresponding to  $\beta = 0$  in (1.1), partially because the infinitesimal generator of the process is related to the fractional Laplacian operator. The operator has many equivalent definitions including singular integrals, the Riesz potential operator, Bochner's subordination and so on [21]. Schertzer *et al.* [30] derived a fractional FPE of nonlinear stochastic differential equations driven by non-Gaussian Lévy stable noises and discussed the existence and uniqueness of the solution. A number of references [34, 37] showed the existence and uniqueness of weak solution for nonlocal Fokker-Planck equations. Huang *et al.* [17] investigated weak and strong maximum principles for a class of general Lévy type Markov generators (nonlocal Waldenfel's operators). The regularity results for the solutions are given in [7, 14, 27].

The numerical methods developed recently for the case include finite differences with quadrature, spectral method, Galerkin finite element method. Using the different definitions of fractional derivatives, Liu *et al.* [22] transformed the space fractional Fokker-Planck equation into ordinary differential equations and solved it by a method of lines. Huang *et al.* [18], Gao *et al.* [11] and Wang *et al.* [35] presented finite difference methods with different quadrature rules in one and two dimensions. Du *et al.* [9, 33] considered the discontinuous and continuous Galerkin methods for certain nonlocal diffusion problems. D'Elia *et al.* [8] used the nonlocal vector calculus to show that the solutions of these nonlocal problems converge to the solutions of fractional Laplacian problems as the domain of the nonlocal interactions becomes infinite. Mao *et al.* [23, 24] developed efficient spectral-Galerkin algorithms for fractional partial differential equations. Recently, Acosta *et al.* [1] dealt with the integral version of the Dirichlet homogeneous fractional Laplace equation and gave a finite element analysis. They also presented high-order numerical methods for one-dimensional fractional-Laplacian boundary value problems [2].

Asymmetric  $\alpha$ -stable Lévy motion is widely applied in physical sciences and economy [15, 20, 32]. Chen *et al.* [5, 6] constructed and proved the existence and the uniqueness of the fundamental solution (heat kernel) of nonsymmetric Lévy-type operator and established its sharp two-sided estimates. Riabiz *et al.* [25] gives the modified Poisson series representation of linear stochastic processes driven by asymmetric stable Lévy process. As the lack of the closed-form density expressions limits its application, we will provide the numerical approximation for the probability density as solution to Fokker-Planck equation. However, to our knowledge, there are few work in developing the numerical methods for the asymmetric case. Zeng *et al.* [39] presented the numerical solution of the space-fractional FPE and studied properties of parameter-induced aperiodic stochastic resonance in the presence of asymmetric Lévy noise.

In our work, we mainly consider the FPE driven by asymmetric Lévy motion, develop a fast

numerical scheme and discuss the properties of the probability density functions. This paper is structured as follows. In section 2, we present the Fokker-Planck equation for a SDE driven by asymmetric  $\alpha$ -stable Lévy motion. In section 3, we show the symmetry of solutions and present the numerical scheme. The numerical solutions and their properties are shown in section 4. Finally, we summarize the results in section 5.

## 2 Fokker-Planck equation driven by stable Lévy motion

Consider the following SDE

$$dX_t = f(X_t)dt + \sigma dB_t + dL_t, \quad X_0 = x. \quad (2.1)$$

where  $f$  is a drift term,  $\sigma$  is non-negative diffusion constant,  $L_t$  is a Lévy motion with the generating triplet  $(\varepsilon K_{\alpha,\beta}, 0, \varepsilon \nu_{\alpha,\beta})$  and  $\nu_{\alpha,\beta}$  is a Lévy jump measure to be defined later. We choose the Lévy motion  $L_t$  such that  $L_1$  is the random variable whose the probability density function(PDF) corresponds to the stable distribution  $S_\alpha(1, \beta, 0)$ . Here,  $\alpha$  ( $0 < \alpha \leq 2$ ) is the index of stability and  $\varepsilon$  is the intensity of Lévy noise.

For every  $\varphi \in H_0^2(\mathbb{R})$ , the generator for the solution of SDE (2.1) is

$$\mathcal{A}\varphi = (f(x) + \varepsilon K_{\alpha,\beta})\varphi_x + \frac{\sigma^2}{2}\varphi_{xx} + \varepsilon \mathcal{L}_{\alpha,\beta}\varphi, \quad (2.2)$$

where

$$\mathcal{L}_{\alpha,\beta}\varphi = \int_{\mathbb{R} \setminus \{0\}} [\varphi(x+y) - \varphi(x) - 1_{\{|y|<1\}}y\varphi'(x)]\nu_{\alpha,\beta}(dy). \quad (2.3)$$

The Fokker-Planck equation for the PDF  $p(x, t)$  of the process  $X_t$  associated with SDE (2.1) is

$$p_t = \mathcal{A}^*p, \quad p(x, 0) = p_0(x), \quad (2.4)$$

where  $\mathcal{A}^*$  is the adjoint operator of  $\mathcal{A}$  in Hilbert space [10], given by

$$\mathcal{A}^*\varphi = -((f + \varepsilon K_{\alpha,\beta})\varphi)_x + \frac{\sigma^2}{2}\varphi_{xx} - \varepsilon \int_{\mathbb{R} \setminus \{0\}} [\varphi(x) - \varphi(x-y) - 1_{\{|y|<1\}}y\varphi'(x)]\nu_{\alpha,\beta}(dy). \quad (2.5)$$

### 2.1 Asymmetric $\alpha$ -stable Lévy motion

In the following, we focus on the FPE driven by asymmetric  $\alpha$ -stable Lévy motion.

The Lévy measure  $\nu_{\alpha,\beta}$  is given by [36]

$$\nu_{\alpha,\beta}(dy) = \frac{C_p 1_{\{0 < y < \infty\}}(y) + C_n 1_{\{-\infty < y < 0\}}(y)}{|y|^{1+\alpha}} dy, \quad (2.6)$$

with

$$C_p = C_\alpha \frac{1+\beta}{2}, \quad C_n = C_\alpha \frac{1-\beta}{2}, \quad -1 \leq \beta \leq 1, \quad (2.7)$$

and

$$C_\alpha = \begin{cases} \frac{\alpha(1-\alpha)}{\Gamma(2-\alpha) \cos(\frac{\pi\alpha}{2})}, & \alpha \neq 1; \\ \frac{2}{\pi}, & \alpha = 1. \end{cases} \quad (2.8)$$

The constant  $K_{\alpha,\beta}$  in (2.2) is given by

$$K_{\alpha,\beta} = \begin{cases} \frac{C_p - C_n}{1-\alpha} = \frac{\beta C_\alpha}{1-\alpha}, & \alpha \neq 1; \\ (\int_1^\infty \frac{\sin(x)}{x^2} dx + \int_0^1 \frac{\sin(x)-x}{x^2} dx)(C_n - C_p), & \alpha = 1. \end{cases} \quad (2.9)$$

Here notice that  $C_p(-\beta) = C_n(\beta)$  and  $K_{\alpha,-\beta} = -K_{\alpha,\beta}$ .

We can rewrite the adjoint operator of  $\mathcal{L}_{\alpha,\beta}$

$$-\mathcal{L}_{\alpha,\beta}^* \varphi(x) = \int_{\mathbb{R} \setminus \{0\}} [\varphi(x) - \varphi(x-y) - 1_{\{|y|<1\}} y \varphi'(x)] \nu_{\alpha,\beta}(dy)$$

as

$$-\mathcal{L}_{\alpha,\beta}^* \varphi(x) = - \int_{\mathbb{R} \setminus \{0\}} [\varphi(x+y) - \varphi(x) - 1_{\{|y|<1\}} y \varphi'(x)] \nu_{\alpha,-\beta}(dy). \quad (2.10)$$

by making the change of integration variable  $y \rightarrow -y$ .

Finally, the adjoint operator of the nonlocal term in Eq. (2.5) is

$$\mathcal{L}_{\alpha,\beta}^* \varphi(x) = \int_{\mathbb{R} \setminus \{0\}} [\varphi(x+y) - \varphi(x) - 1_{\{|y|<1\}} y \varphi'(x)] \nu_{\alpha,-\beta}(dy). \quad (2.11)$$

For numerical computations, we change  $1_{\{|y|<1\}}$  to  $1_{\{|y|<b\}}$  in (2.11). Then, the Fokker-Planck equation driven by the asymmetric Lévy motion becomes

$$p_t = -(c(x)p)_x + \frac{\sigma^2}{2} p_{xx} + \varepsilon \int_{\mathbb{R} \setminus \{0\}} [p(x+y, t) - p(x, t) - 1_{\{|y|<b\}} y p_x] \nu_{\alpha,-\beta}(dy), \quad (2.12)$$

where

$$c(x) = \begin{cases} f(x) + \varepsilon K_{\alpha,\beta} + \varepsilon(C_p - C_n) \frac{b^{1-\alpha}-1}{1-\alpha}, & \alpha \neq 1; \\ f(x) + \varepsilon K_{\alpha,\beta} + \varepsilon(C_p - C_n) \ln b, & \alpha = 1, \end{cases} \quad (2.13)$$

with the constants  $C_p$  and  $C_n$  defined by (2.7).

**Remark 2.1.** If  $\beta = 0$ , the process  $L_t$  becomes symmetric Lévy motion, then  $c(x) = f(x)$ ,  $\nu_{\alpha,-\beta}(dy) = \frac{C_\alpha}{|y|^{1+\alpha}} dy$  and  $\mathcal{L}_{\alpha,\beta}$  is self-adjoint.

## 2.2 Auxiliary conditions

For the solution of Eq. (2.12), we specify auxiliary conditions. There are several various boundary conditions for Brownian motion, such as reflecting barrier, absorbing barrier, periodic boundary condition and so on [12]. We consider two cases of processes governed by the SDE (2.1). One is that the process  $X_t$  disappears or is killed when  $X_t$  is outside a bounded domain  $D = (-b, b)$ . In this case, we have the absorbing condition, i.e. the probability  $p(x, t)$  of being outside of the bounded domain  $D = (-b, b)$  is zero:

$$p(x, t) = 0, \quad x \notin (-b, b). \quad (2.14)$$

We can also extend the domain to general unsymmetric domains.

The other case is that the process  $X_t$  can go anywhere on the entire real line  $\mathbb{R}$ . In this case, we call it the natural condition. The probability density satisfies

$$\int_{-\infty}^{\infty} p(x, t) dx = 1, \quad \forall t \geq 0.$$

### 3 Numerical schemes

#### 3.1 Simplification

First, we show the following symmetry for the solution of FPE (2.12).

**Proposition 3.1** (Symmetry of Solutions). *If  $f(x)$  is an odd function and the domain  $D$  is symmetric ( $D = (-b, b)$ ), then the solution  $p(x, t)$  of the Fokker-Planck equation (2.12) is symmetric about the origin for any given time  $t$  if  $\beta$  changes the sign, i.e.  $p(-x, t; -\beta) = p(x, t; \beta)$  for all  $x \in (-b, b)$  where  $p(x, t; \beta)$  and  $p(x, t; -\beta)$  denote the solutions corresponding to  $\beta$  and  $-\beta$  respectively.*

*Proof.* From the Eq. (2.12),  $p(-x, t; -\beta)$  satisfies

$$\begin{aligned} p_t(-x, t; -\beta) &= -(cp)_x(-x, t; -\beta) + \frac{\sigma^2}{2} p_{xx}(-x, t; -\beta) \\ &\quad + \varepsilon \int_{\mathbb{R} \setminus \{0\}} [p(-x + y, t; -\beta) - p(-x, t; -\beta) - 1_{\{|y| < b\}} y p_x(-x, t; -\beta)] \nu_{\alpha, \beta}(dy). \end{aligned} \quad (3.1)$$

By the definition of  $c(x)$  in (2.12), we have  $c(-x; -\beta) = -c(x; \beta)$  if  $f(x)$  is an odd function. Denote  $\tilde{p}(x, t) = p(-x, t; -\beta)$ , then

$$\tilde{p}_x(x, t) = -p_x(-x, t; -\beta), \quad \tilde{p}_{xx}(x, t) = p_{xx}(-x, t; -\beta). \quad (3.2)$$

Taking  $y' = -y$ , we have

$$\begin{aligned} &\int_{\mathbb{R} \setminus \{0\}} [p(-x + y, t; -\beta) - p(-x, t; -\beta) - I_{\{|y| < b\}}(y) y p_x(-x, t; -\beta)] \nu_{\alpha, \beta}(dy) \\ &= \int_{\mathbb{R} \setminus \{0\}} [\tilde{p}(x - y, t) - \tilde{p}(x, t) + I_{\{|y| < b\}}(y) y \tilde{p}_x(x, t)] \left[ \frac{C_p 1_{\{0 < y < \infty\}} + C_n 1_{\{-\infty < y < 0\}}}{|y|^{1+\alpha}} \right] dy \\ &= \int_{\mathbb{R} \setminus \{0\}} [\tilde{p}(x + y', t) - \tilde{p}(x, t) - I_{\{|y'| < b\}}(y') y' \tilde{p}_x(x, t)] \nu_{\alpha, -\beta}(dy'). \end{aligned} \quad (3.3)$$

From the property of  $c(x)$ , Eqs. (3.1) and (3.3), we finally have

$$\begin{aligned} \tilde{p}_t(x, t) &= -(c(x; \beta)\tilde{p}(x, t))_x + \frac{\sigma^2}{2} \tilde{p}_{xx}(x, t) \\ &\quad + \varepsilon \int_{\mathbb{R} \setminus \{0\}} [\tilde{p}(x + y, t) - \tilde{p}(x, t) - 1_{\{|y| < b\}} y \tilde{p}_x(x, t)] \nu_{\alpha, -\beta}(dy) \end{aligned} \quad (3.4)$$

Then, we get the conclusion by the uniqueness of the solution to (2.12). □

For convenience, we convert the domain  $D = (-b, b)$  to the standard domain  $(-1, 1)$  by the variable transformation

$$s = x/b, \quad \text{and } v(s, t) := p(bs, t). \quad (3.5)$$

Then, Eq. (2.12) changes to

$$\begin{aligned} v_t &= -\frac{1}{b} (c(bs)v)_s + \frac{\sigma^2}{2b^2} v_{ss} \\ &\quad + \varepsilon b^{-\alpha} \int_{\mathbb{R} \setminus \{0\}} [v(s + r, t) - v(s, t) - I_{\{|r| < 1\}}(r) r v_s(s, t)] \left[ \frac{C_n 1_{\{0 < r < \infty\}} + C_p 1_{\{-\infty < r < 0\}}}{|r|^{1+\alpha}} \right] dr. \end{aligned} \quad (3.6)$$

Next, we present the numerical schemes for the absorbing boundary condition. By using the absorbing boundary condition, i.e. the probability density  $v(x, t)$  vanish outside of the standard domain  $D = (-1, 1)$ . The above equation (3.6) containing the singular integral is simplified to the following equations [36].

For  $s < 0$ ,

$$\begin{aligned} v_t = & \frac{\sigma^2}{2b^2}v_{ss} - \frac{1}{b}(c(bs)v)_s + \varepsilon b^{-\alpha}C_p g(s)v_s - \varepsilon b^{-\alpha}\frac{v}{\alpha} \left[ \frac{C_n}{(1-s)^\alpha} + \frac{C_p}{(1+s)^\alpha} \right] \\ & + \varepsilon b^{-\alpha}C_n \int_0^1 \frac{v(s+y, t) - v(s, t) - yv_s(s, t)}{y^{1+\alpha}} dy + \varepsilon b^{-\alpha}C_n \int_1^{1-s} \frac{v(s+y, t) - v(s, t)}{y^{1+\alpha}} dy \\ & + \varepsilon b^{-\alpha}C_p \int_0^{1+s} \frac{v(s-y, t) - v(s, t) + yv_s(s, t)}{y^{1+\alpha}} dy; \end{aligned} \quad (3.7)$$

For  $s \geq 0$ ,

$$\begin{aligned} v_t = & \frac{\sigma^2}{2b^2}v_{ss} - \frac{1}{b}(c(bs)v)_s - \varepsilon b^{-\alpha}C_n g(s)v_s - \varepsilon b^{-\alpha}\frac{v}{\alpha} \left[ \frac{C_n}{(1-s)^\alpha} + \frac{C_p}{(1+s)^\alpha} \right] \\ & + \varepsilon b^{-\alpha}C_n \int_0^{1-s} \frac{v(s+y, t) - v(s, t) - yv_s(s, t)}{y^{1+\alpha}} dy + \varepsilon b^{-\alpha}C_p \int_1^{1+s} \frac{v(s-y, t) - v(s, t)}{y^{1+\alpha}} dy \\ & + \varepsilon b^{-\alpha}C_p \int_0^1 \frac{v(s-y, t) - v(s, t) + yv_s(s, t)}{y^{1+\alpha}} dy. \end{aligned} \quad (3.8)$$

Here,

$$g(s) = \begin{cases} \frac{1-(1-|s|)^{1-\alpha}}{1-\alpha}, & \alpha \neq 1; \\ -\ln(1-|s|), & \alpha = 1. \end{cases} \quad (3.9)$$

Assuming the drift term  $f$  is differentiable, we change the Eqs. (3.7) and (3.8) to the following.

For  $s < 0$ ,

$$\begin{aligned} v_t = & \frac{\sigma^2}{2b^2}v_{ss}(s, t) - m_1(s)v_s(s, t) - m_2(s)v(s, t) \\ & + \varepsilon b^{-\alpha}C_n \int_0^1 \frac{v(s+y, t) - v(s, t) - yv_s(s, t)}{y^{1+\alpha}} dy + \varepsilon b^{-\alpha}C_n \int_1^{1-s} \frac{v(s+y, t) - v(s, t)}{y^{1+\alpha}} dy \\ & + \varepsilon b^{-\alpha}C_p \int_0^{1+s} \frac{v(s-y, t) - v(s, t) + yv_s(s, t)}{y^{1+\alpha}} dy; \end{aligned} \quad (3.10)$$

for  $s \geq 0$ ,

$$\begin{aligned} v_t = & \frac{\sigma^2}{2b^2}v_{ss}(s, t) - m_1(s)v_s(s, t) - m_2(s)v(s, t) \\ & + \varepsilon b^{-\alpha}C_n \int_0^{1-s} \frac{v(s+y, t) - v(s, t) - yv_s(s, t)}{y^{1+\alpha}} dy + \varepsilon b^{-\alpha}C_p \int_1^{1+s} \frac{v(s-y, t) - v(s, t)}{y^{1+\alpha}} dy \\ & + \varepsilon b^{-\alpha}C_p \int_0^1 \frac{v(s-y, t) - v(s, t) + yv_s(s, t)}{y^{1+\alpha}} dy. \end{aligned} \quad (3.11)$$

where

$$m_1(s) = \begin{cases} \frac{c(bs)}{b} - \varepsilon b^{-\alpha}C_p g(s), & s < 0; \\ \frac{c(bs)}{b} + \varepsilon b^{-\alpha}C_n g(s), & s \geq 0, \end{cases} \quad (3.12)$$

and

$$m_2(s) = c'(bs) + \frac{\varepsilon b^{-\alpha}}{\alpha} \left[ \frac{C_n}{(1-s)^\alpha} + \frac{C_p}{(1+s)^\alpha} \right]. \quad (3.13)$$

### 3.2 Discretization

We aim to solve the FPE (3.10) and (3.11) numerically. First, we denote  $V_j$  as the numerical solution of  $v$  at  $(s_j, t)$ , where  $s_j = jh$  for  $j \in \mathbb{Z}$  and  $h = \frac{1}{J}$ . Due to the absorbing condition,  $V_j = 0$  for  $|j| \leq J$  and we denote the unknowns  $V_j$  for  $-J < j < J$  by the vector  $\mathbf{V} := (V_{-J+1}, V_{-J+2}, \dots, V_{J-1})^T$ . Second, we approximate the diffusion term by the second-order central differencing and the first-order derivatives by the first-order upwind scheme. Denoting

$$\delta_u V_j = \begin{cases} \frac{V_j - V_{j-1}}{h}, & \text{if } m_1(s_j) > 0; \\ \frac{V_{j+1} - V_j}{h}, & \text{if } m_1(s_j) < 0, \end{cases} \quad (3.14)$$

we discretize the non-integral terms in the RHS of Eqs. (3.10) and (3.11) as

$$(B\mathbf{V})_j := C_h \frac{V_{j+1} - 2V_j + V_{j-1}}{h^2} - m_1(s_j) \delta_u V_j - m_2(s_j) V_j, \quad (3.15)$$

where

$$C_h = \frac{\sigma^2}{2b^2} - \frac{\varepsilon b^{-\alpha}}{2} C_\alpha \zeta(\alpha - 1) h^{2-\alpha}. \quad (3.16)$$

The second term in  $C_h$  is the leading-order correction term for the trapezoidal rules of the singular integrals in Eqs. (3.10) and (3.11) given below, and  $\zeta$  is the Riemann zeta function. Eq. (3.15) defines a linear operator or a  $(2J - 1)$ -by- $(2J - 1)$  matrix  $B$ .

Third, the integrals in Eqs. (3.10) and (3.11) are approximated by the trapezoidal rule

$$(S\mathbf{V})_j := \begin{cases} \varepsilon b^{-\alpha} C_n h \sum'_{k=j+1}^{J+j} \frac{V_k - V_j - (s_k - s_j) \frac{V_j - V_{j-1}}{h}}{(s_k - s_j)^{\alpha+1}} + \varepsilon b^{-\alpha} C_n h \sum_{k=J+j}^J \frac{V_k - V_j}{(s_k - s_j)^{1+\alpha}} \\ + \varepsilon b^{-\alpha} C_p h \sum_{k=-J}^{j-1} \frac{V_k - V_j - (s_k - s_j) \frac{V_{j+1} - V_j}{h}}{(s_j - s_k)^{\alpha+1}}, & \text{for } -J + 1 \leq j \leq -1, \\ \varepsilon b^{-\alpha} C_n h \sum'_{k=j+1}^J \frac{V_k - V_j - (s_k - s_j) \frac{V_j - V_{j-1}}{h}}{(s_k - s_j)^{\alpha+1}} + \varepsilon b^{-\alpha} C_p h \sum_{k=-J}^{-J+j} \frac{V_k - V_j}{(s_j - s_k)^{1+\alpha}} \\ + \varepsilon b^{-\alpha} C_p h \sum_{k=-J+j}^{j-1} \frac{V_k - V_j - (s_k - s_j) \frac{V_{j+1} - V_j}{h}}{(s_j - s_k)^{\alpha+1}}, & \text{for } 0 \leq j \leq J - 1. \end{cases} \quad (3.17)$$

The summation symbol  $\sum$  means the terms of both end indices are multiplied by  $\frac{1}{2}$ ,  $\sum'$  ( $\sum''$ ) means that only the term of the top (bottom) index is multiplied by  $\frac{1}{2}$ . Eq. (3.17) defines another linear operator or  $(2J - 1)$ -by- $(2J - 1)$  matrix  $S$ . Note the trapezoidal rule in (3.17) would induce significant error due to the singular nature of the integrals and the dominant error is eliminated by the second term in (3.16). [31, 36]

Now, we present our semi-discrete scheme for solving the FPE (3.10) and (3.11)

$$\frac{dV_j}{dt} = (A\mathbf{V})_j, \quad \text{where } A := B + S, \quad (3.18)$$

for  $-J + 1 \leq j \leq J - 1$ .

**Remark 3.1.** We point out that our semi-discrete scheme for the natural condition will be the same as (3.18) except  $m_2(s)$  simplifies to  $c'(bs)$ .

### 3.3 Fast Algorithm

The summation terms in the discretized scheme (3.18) can be written in matrix-vector multiplication form  $S\mathbf{V}$  as given by (3.17). We decompose the matrix  $S$  as the summation of a Toeplitz matrix  $T_S$  and a tridiagonal matrix  $D_S$

$$S = T_S + D_S, \quad (3.19)$$

where

$$T_S = \begin{pmatrix} 0 & \frac{\tilde{C}_n}{h^{1+\alpha}} & \frac{\tilde{C}_n}{(2h)^{1+\alpha}} & \cdots & \frac{\tilde{C}_n}{[(2J-2)h]^{1+\alpha}} \\ \frac{\tilde{C}_p}{h^{1+\alpha}} & 0 & \frac{\tilde{C}_n}{h^{1+\alpha}} & \cdots & \frac{\tilde{C}_n}{[(2J-3)h]^{1+\alpha}} \\ \frac{\tilde{C}_p}{(2h)^{1+\alpha}} & \frac{\tilde{C}_p}{h^{1+\alpha}} & 0 & \ddots & \frac{\tilde{C}_n}{[(2J-4)h]^{1+\alpha}} \\ \vdots & \vdots & \ddots & \ddots & \vdots \\ \frac{\tilde{C}_p}{[(2J-2)h]^{1+\alpha}} & \frac{\tilde{C}_p}{[(2J-3)h]^{1+\alpha}} & \frac{\tilde{C}_p}{[(2J-4)h]^{1+\alpha}} & \cdots & 0 \end{pmatrix}, \quad (3.20)$$

$$D_S = \begin{pmatrix} a_1 & p_1 & & & \\ b_2 & a_2 & p_2 & & \\ & \ddots & \ddots & \ddots & \\ & & b_{2J-2} & a_{2J-2} & p_{2J-2} \\ & & & b_{2J-1} & a_{2J-1} \end{pmatrix}. \quad (3.21)$$

Here

$$\tilde{C}_p = \varepsilon b^{-\alpha} C_p h, \quad \tilde{C}_n = \varepsilon b^{-\alpha} C_n h, \quad (3.22)$$

and

$$\begin{aligned} a_{J+j} &= -\tilde{C}_n \left[ \sum'_{k=j+1}^J \frac{1}{(s_k - s_j)^{\alpha+1}} \right] - \tilde{C}_p \left[ \sum''_{k=-J}^{j-1} \frac{1}{(s_j - s_k)^{\alpha+1}} \right] \\ &- \begin{cases} \frac{\tilde{C}_n}{h} \sum'_{k=j+1}^{J+j} \frac{1}{(s_k - s_j)^\alpha} + \frac{\tilde{C}_p}{h} \sum''_{k=-J}^{j-1} \frac{1}{(s_j - s_k)^\alpha}, & \text{for } j = 1 - J, 2 - J, \dots, 0, \\ \frac{\tilde{C}_n}{h} \sum'_{k=j+1}^J \frac{1}{(s_k - s_j)^\alpha} + \frac{\tilde{C}_p}{h} \sum''_{k=-J+j}^{j-1} \frac{1}{(s_j - s_k)^\alpha}, & \text{for } j = 1, J + 2, \dots, J - 1, \end{cases} \\ p_{J+j} &= \begin{cases} \frac{\tilde{C}_p}{h} \sum''_{k=-J}^{j-1} \frac{1}{(s_j - s_k)^\alpha}, & \text{for } j = 1 - J, 2 - J, \dots, 0, \\ \frac{\tilde{C}_p}{h} \sum''_{k=-J+j}^{j-1} \frac{1}{(s_j - s_k)^\alpha}, & \text{for } j = 1, 2, \dots, J - 1, \end{cases} \\ b_{J+j} &= \begin{cases} \frac{\tilde{C}_n}{h} \sum'_{k=j+1}^{J+j} \frac{1}{(s_k - s_j)^\alpha}, & \text{for } j = 1 - J, 2 - J, \dots, 0, \\ \frac{\tilde{C}_n}{h} \sum'_{k=j+1}^J \frac{1}{(s_k - s_j)^\alpha}, & \text{for } j = 1, 2, \dots, J - 1. \end{cases} \end{aligned}$$

The direct summation of  $S\mathbf{V}$  causes the computational complexity of the scheme (3.18) to be  $O(J^2)$ . Realizing that the dominant computational cost comes from Toeplitz matrix-vector multiplications, we develop our fast algorithm based on the well-known algorithm of  $O(J \log J)$  for multiplying a vector by a Toeplitz matrix [13].

Next, we compare the CPU times using fast algorithm with those using direct summation in Table 1 for the case of  $\alpha = 0.5, \beta = 0.5, f \equiv 0, d = 0, \varepsilon = 1$  with  $\Delta t = \frac{1}{1600}$  and different resolutions  $J$  from time 0 to  $t_F = 1$ . The initial condition is a Gaussian density function  $p(x, 0) = \sqrt{\frac{40}{\pi}} e^{-40x^2}$ . The numerical schemes, implemented in MATLAB, were executed on a desktop PC with 3.6 GHz Intel Core i7-4790 processor and 8GB RAM.

From the results in Table 1, the CPU time for the scheme with the fast algorithm increases as  $O(J \log J)$  while the scheme with the direct summation grows quadratically in  $J$ . This behavior agrees with the theoretical analysis of the complexity of the algorithms.



## 4 Maximum principle

In this section, we will show that the semi-discrete scheme (3.18) satisfies the discrete maximum principle under the condition the function  $m_2(s)$  defined in (3.13) is non-negative for  $|s| < 1$ : the solution to (3.18) reaches its maximum and minimum outside the solution domain, i.e. in  $\partial I_{h,t_F}$  defined in

$$I_h = \{j \in \mathbb{Z} : |jh| < 1\}, \quad I_{h,t_F} = I_h \times (0, t_F], \quad \partial I_{h,t_F} = \mathbb{Z} \times [0, t_F] \setminus I_{h,t_F}, \quad (4.1)$$

where  $t_F > 0$  is any fixed final time. We point out the unusual definition of the "boundary" of the solution domain due to the nonlocal exterior absorbing condition (2.14). For weak and strong maximum principles for the original equation (2.4) or nonlocal Waldenfels operator, we refer to the work [17].

**Proposition 4.1** (Maximum principle for the absorbing condition). *Assume  $m_2(s) \geq 0$  for  $s \in (-1, 1)$ .*

(i) If

$$\frac{dV_j}{dt} - (A\mathbf{V})_j \leq 0 \text{ for } (j, t) \in I_{h,t_F} \quad \text{and} \quad V_j = 0 \text{ for } |j| \geq J, \quad (4.2)$$

then

$$\max_{(j,t) \in \mathbb{Z} \times [0, t_F]} V_j(t) = \max_{(j,t) \in \partial I_{h,t_F}} V_j(t). \quad (4.3)$$

(ii) If

$$\frac{dV_j}{dt} - (A\mathbf{V})_j \geq 0 \text{ for } (j, t) \in I_{h,t_F} \quad \text{and} \quad V_j = 0 \text{ for } |j| \geq J, \quad (4.4)$$

then

$$\min_{(j,t) \in \mathbb{Z} \times [0, t_F]} V_j(t) = \min_{(j,t) \in \partial I_{h,t_F}} V_j(t). \quad (4.5)$$

*Proof.* 1. Let us suppose

$$\frac{dV_j}{dt} - (A\mathbf{V})_j < 0 \text{ for } (j, t) \in I_{h,t_F} \quad \text{and} \quad V_j = 0 \text{ for } |j| \geq J, \quad (4.6)$$

but there exist a point  $(j^*, t^*) \in I_{h,t_F}$  such that  $V_{j^*}(t^*) = \max_{\mathbb{Z} \times [0, t_F]} V_j$ .

2. If  $0 < t^* < t_F$ , then

$$\frac{dV_{j^*}}{dt} = 0 \text{ at } t = t^*. \quad (4.7)$$

On the other hand, we have, at  $t = t^*$ ,  $(s_k - s_{j^*}) \frac{V_{j^*} - V_{j^*-1}}{h} \geq 0$  for  $j^* + 1 \leq k \leq J$  and  $(s_k - s_{j^*}) \frac{V_{j^*+1} - V_{j^*}}{h} \geq 0$  for  $-J \leq k \leq j^* - 1$  because  $V_{j^*}(t^*)$  is the maximum. Consequently, each summation term in (3.17) is non-positive, resulting  $(S\mathbf{V})_{j^*} \leq 0$  at  $t = t^*$ . Due to the fact that  $V_{j^*}(t^*)$  is the maximum,  $V_{j^*+1} - 2V_{j^*} + V_{j^*-1} \leq 0$ ,  $m_1(s_{j^*})\delta_u V_{j^*} \geq 0$  from the upwind

$J$	100	200	400	800
CPU times (sec) with direct summation	15.85	50.99	179.25	671.47
CPU times (sec) using the fast algorithm	0.13	0.16	0.34	0.79

Table 1: Comparison of the CPU times of computing the solution of the FPE with and without the fast algorithm for the case  $\alpha = 0.5, \beta = 0.5, f \equiv 0, d = 0, \varepsilon = 1$  and different  $J$ 's.

scheme (3.14),  $m_2(s_{j^*})V_{j^*} \geq 0$  from the assumption  $m_2(s) \geq 0$  and  $V_{j^*} \geq 0 = V_k$  for  $k \geq J$ , resulting  $(B\mathbf{V})_{j^*} \leq 0$  at  $t = t^*$ . Therefore, together with (4.7), we have  $\frac{dV_{j^*}}{dt} - (A\mathbf{V})_{j^*} \geq 0$  at  $t = t^*$ , which is a contradiction to (4.6).

3. If  $t^* = t_F$ , then  $\frac{dV_{j^*}}{dt} \geq 0$  at  $t = t^*$  because  $V_j$  reaches its maximum at  $(j^*, t^*)$  for all  $(j, t) \in \mathbb{Z} \times [0, t_F]$ . The argument in the previous point 2 still holds, i.e.,  $(A\mathbf{V})_{j^*} \leq 0$  at  $t = t^*$ . Thus, it is a contradiction to (4.6).
4. In the general case of (4.2), we define  $\mathbf{V}^\delta := \mathbf{V} - \delta t$  where  $\delta$  is a positive parameter. Then, we have  $A\mathbf{V}^\delta = A\mathbf{V}$ , and  $\frac{dV_j^\delta}{dt} - (A\mathbf{V}^\delta)_j = \frac{dV_j}{dt} - \delta - (A\mathbf{V})_j < 0$  for  $(j, t) \in I_{h, t_F}$ . Thus, we have  $\max_{(j, t) \in \mathbb{Z} \times [0, t_F]} V_j^\delta(t) = \max_{(j, t) \in \partial I_{h, t_F}} V_j^\delta(t)$ . We obtain (4.3) by letting  $\delta \rightarrow 0$ . This concludes the proof of the assertion (i).
5. By considering  $-\mathbf{V}$ , the assertion (ii) follows immediately. □

**Remark 4.1.** *The condition  $m_2 \geq 0$  for the maximum principle is equivalent to requiring the drift  $f$  satisfy  $f' \geq -\min_{s \in (-1, 1)} \frac{\varepsilon b^{-\alpha}}{\alpha} [\frac{C_n}{(1-s)^\alpha} + \frac{C_p}{(1+s)^\alpha}]$ . For example, if  $\alpha = \beta = 0.5, \varepsilon = 1, b = 1$ , the RHS of the above inequality is  $-0.76$ , therefore, the O-U potential  $f = -0.6x$  would satisfy the maximum principle. We point out that any drift  $f$  with  $f' \geq 0$  satisfies the condition  $m_2 \geq 0$ .*

**Proposition 4.2** (Maximum principle for the natural condition). *Assume  $f'(bs) \geq 0$  for  $s \in (-1, 1)$ .*

(i) *If*

$$\frac{dV_j}{dt} - (A\mathbf{V})_j \leq 0 \text{ for } (j, t) \in I_{h, t_F}, \quad (4.8)$$

*then*

$$\max_{(j, t) \in \mathbb{Z} \times [0, t_F]} V_j(t) = \max_{(j, t) \in \partial I_{h, t_F}} V_j(t). \quad (4.9)$$

(ii) *If*

$$\frac{dV_j}{dt} - (A\mathbf{V})_j \geq 0 \text{ for } (j, t) \in I_{h, t_F} \quad (4.10)$$

*then*

$$\min_{(j, t) \in \mathbb{Z} \times [0, t_F]} V_j(t) = \min_{(j, t) \in \partial I_{h, t_F}} V_j(t). \quad (4.11)$$

*Proof.* We note that the numerical scheme for the natural condition is the same as that for the absorbing condition except the definition of  $m_2$  is simplified to  $c'(bs)$  or  $f'(bs)$  (see Remark 3.1 and Eq. (2.13)). Consequently, the proof is the same as that for Proposition 4.1. □

**Remark 4.2.** *One can find many fully discrete schemes that satisfies maximum principle. For example, one can show that, if  $m_2(s) \geq 0$  for  $s \in (-1, 1)$ , then the solution to the backward Euler scheme for the time integration*

$$\frac{V_j^n - V_j^{n-1}}{\Delta t} = (A\mathbf{V}^n)_j, \quad \text{for } -J+1 \leq j \leq J-1, \quad n = 1, 2, \dots \quad (4.12)$$

*where  $V_j^n$  means the numerical solution of  $v$  at  $(s_j, t_n)$  with  $t_n = n\Delta t$  and  $\mathbf{V}^n = (V_{-J+1}^n, \dots, V_{J-1}^n)^T$ , satisfies the maximum principle*

$$\max_{(j, n) \in I_h \times I_n} V_j^n \leq \max_{(j, n) \in \mathbb{Z} \times I_n \setminus I_h \times I_n} V_j^n, \quad \min_{(j, n) \in I_h \times I_n} V_j^n \geq \min_{(j, n) \in \mathbb{Z} \times I_n \setminus I_h \times I_n} V_j^n, \quad (4.13)$$

where  $\Delta t = t_F/n_F$  for some total number of time steps  $n_F \in \mathbb{Z}$  and

$$I_n = \{n \in \mathbb{Z} : 1 \leq n \leq n_F\}, \quad \bar{I}_n = \{n \in \mathbb{Z} : 0 \leq n \leq n_F\}. \quad (4.14)$$

The proof will follow closely with that for Proposition 4.1 by realizing that, if  $V_j^n$  reaches the maximum at  $V_{j^*}^{n^*}$ , then

$$\frac{V_{j^*}^{n^*} - V_{j^*}^{n^*-1}}{\Delta t} \geq 0. \quad (4.15)$$

In the following, we mainly use the backward Euler for time evolution as the probability density will be negative near the boundary for the forward Euler scheme. The Fig. 1 shows the situation for  $\alpha = 0.5, \beta = 0.5, f = -x, \sigma = 0, \varepsilon = 1$ .

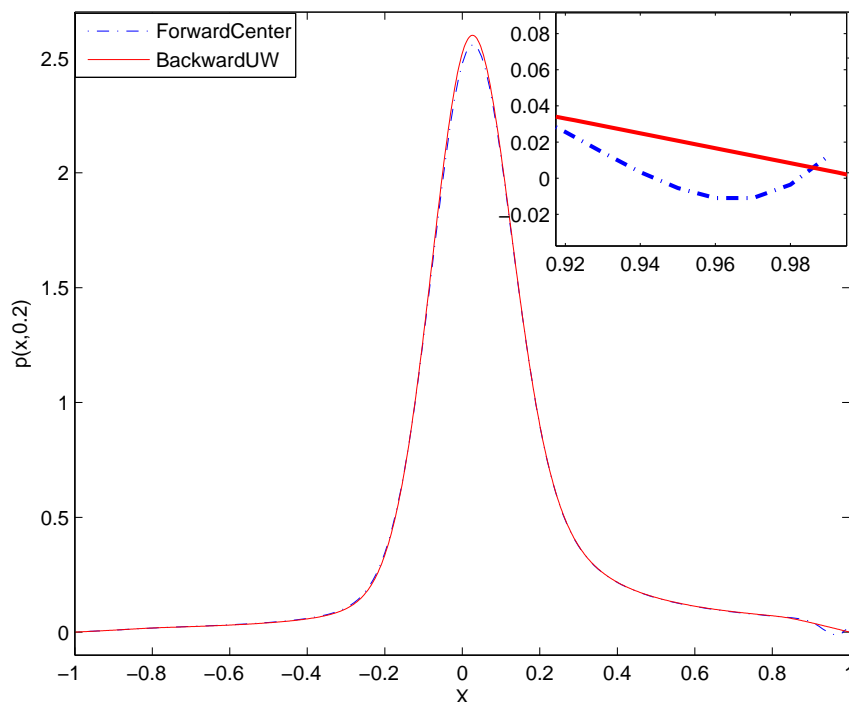


Figure 1: Different numerical scheme for FPE with  $\alpha = 0.5, \beta = 0.5, f = -x, \sigma = 0, \varepsilon = 1$ . The blue solid line provide the numerical solution for time evolution with forward Euler(blue solid line) and backward Euler(red dash-dot line).

**Remark 4.3.** *The stability of the schemes based on (3.18) follows immediately from the maximum principle we have proved in the section. It is obvious that the fully discretized schemes are consistent, where the details of the truncation error is discussed in [36]. Since the equations (3.10) and (3.11) are linear, the schemes are convergent due to the Lax Equivalence theorem.*

## 5 Numerical results

### 5.1 Verification

Before discussing the evolution of the PDFs obtained from the simulations, we validate our numerical methods by comparing with a known exact solution. Based on the density function for Lévy

distribution( $\alpha = 0.5, \beta = 1$ ) and the scaling property of stable random variables, we have the PDF for  $L_t$  [3, 10, 28]

$$p(x, t) = \frac{x^{-\frac{3}{2}} t}{\sqrt{2\pi}} e^{-\frac{t^2}{2x}}, \quad \text{for } x > 0; \quad p(x, t) = 0, \quad \text{for } x \leq 0. \quad (5.1)$$

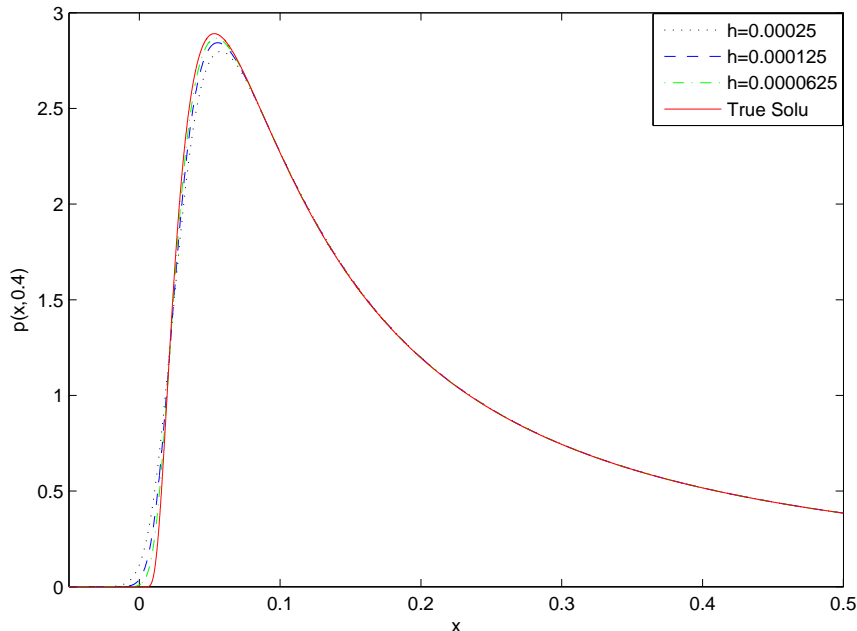


Figure 2: Comparison between the analytic solution (the solid line) and the numerical solutions at time  $t_F = 0.4$  for  $\alpha = 0.5, \beta = 1, f \equiv 0, \sigma = 0, \varepsilon = 1$  and different resolutions  $h = 0.00025$  (the dotted line),  $0.000125$  (the dashed line) and  $0.0000625$  (the dash-dotted line).

To compare our numerical solution with the exact solution (5.1), we start our numerical computation from the time  $t = 0.2$  by setting the initial condition to be  $p(x, 0.2)$  given in (5.1). Noticing the analytic solution correspond to the natural condition, we take the computational domain  $D = (-10, 10)$  and  $\alpha = 0.5, \beta = 1, f \equiv 0, \sigma = 0, \varepsilon = 1$ . Figure 2 shows the solutions at the time  $t_F = 0.4$  with different spatial resolutions  $h = 0.00025, 0.000125, 0.0000625$  and the time step-size  $\Delta t = 0.5h$ . The results show that the numerical solutions agree with the exact solution well and the difference or the error decreases as we increase the resolution.

## 5.2 Evolution of PDFs

One of the ways to understand the behavior of a stochastic process governed by the SDE (2.1) is through its PDF. First, we numerically find the PDF corresponding to  $L_t$  subject to the absorbing condition with  $D = (-1, 1)$ . Initially, the location of the process is at  $x$  has the probability  $p(x, 0) = \sqrt{\frac{40}{\pi}} e^{-40x^2}$ , having a sharp peak at the origin 0. The time evolution of the probability density  $p$  is shown in Fig. 3 for  $f \equiv 0, \sigma = 0, \beta = 0.5, \varepsilon = 1$  and two different values of  $\alpha = 0.5, 1.5$ . For  $\alpha = 0.5$ , the peak decays and moves to the right; for  $\alpha = 1.5$ , the peak decays faster but moves to the left. Because the skewness parameter  $\beta$  is positive, there is larger tendency to jump to the right. The linear drift coefficient  $K_{\alpha, \beta}$  due to the compensation is positive when  $\alpha < 1$  and becomes negative when  $\alpha > 1$ . The jump direction and the drift work together to render the movement of the peak in the case of  $\alpha = 0.5$ . On the other hand, when  $\alpha = 1.5$ , the two factors compete and

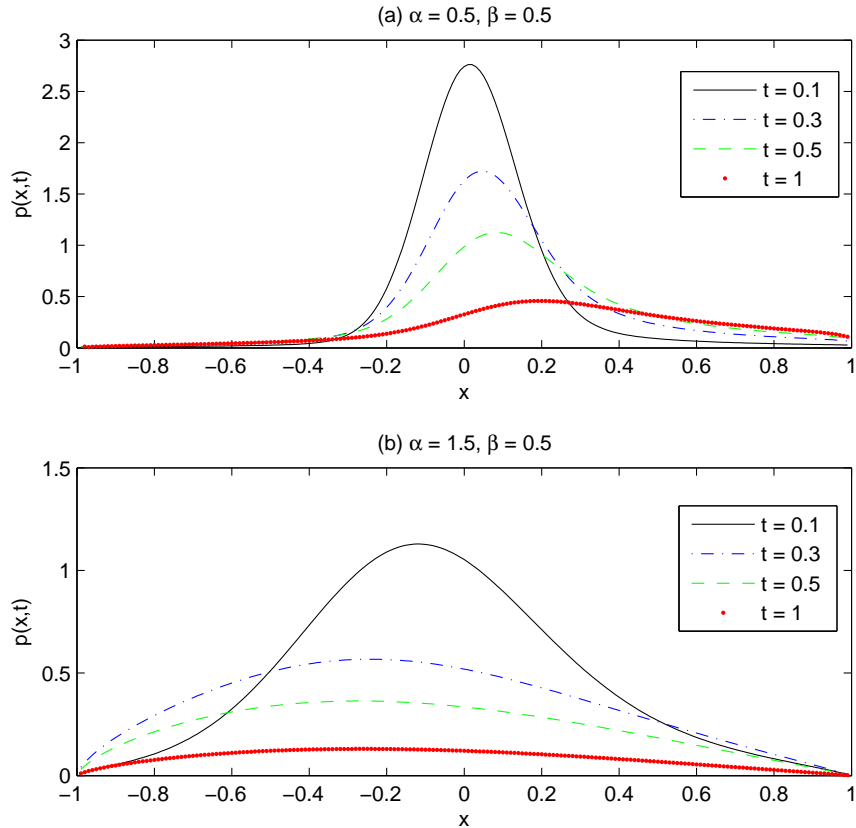


Figure 3: The evolution of PDFs  $p$  for  $\sigma = 0, f \equiv 0, \beta = 0.5, \varepsilon = 1$  subject to the absorbing condition with  $D = (-1, 1)$  and the initial condition  $p(x, 0) = \sqrt{\frac{40}{\pi}}e^{-40x^2}$ . (a)  $\alpha = 0.5$ ; (b)  $\alpha = 1.5$ .

the effect of the drift dominates. Further more, we note that the shape of the PDF becomes convex after  $t \geq 0.3$  and more smooth for  $\alpha = 1.5$ , while the PDF for  $\alpha = 0.5$  appears to be discontinuous at the right boundary  $x = 1$  at large times.

Next, we investigate the effects of different parameters on the solution to the FPE (2.4), including the skewness parameter  $\beta$ , the drift  $f$ , the intensities of Gaussian noise  $\sigma$  and non-Gaussian noise  $\varepsilon$ , the domain size  $D$  and the auxiliary conditions.

We consider the effect of the skewness parameter  $\beta$  on the PDFs with initial condition of a uniform distribution  $p(x, 0) = 0.5I_{\{|x| < 1\}}$  in Fig. 4. The impact of  $\beta$  on the PDF is different for  $0 < \alpha < 1$  and  $1 < \alpha < 2$ . For  $\alpha = 0.5$  (Fig. 4(a)), the PDFs have relatively flat profiles in the middle but drop to zero sharply at the left boundary of the domain  $x = -1$ . As  $\beta$  increases, the probability profile tilts toward the right, i.e., having larger probability for positive  $x$ . We point out the interesting behavior of the PDFs at the right boundary of the domain, where  $p(x, 0.1)$  becomes increasingly discontinuous as  $\beta$  approaches 1. On the other hand, for  $\alpha = 1.5$  (Fig. 4(b)), the profiles of the PDFs are much smoother than those of  $\alpha < 1$  and the values of the PDFs are larger near the left boundary as  $\beta$  increases. It is interesting to note that the PDFs for  $\beta > 0$  reach their maxima at small positive  $x$  values. Similar effects of  $\beta$  can be seen from another example shown in Fig. 5 where the initial condition is a Gaussian distribution  $p(x, 0) = \sqrt{\frac{40}{\pi}}e^{-40x^2}$ . As  $\beta$  increases, the hump in the PDF profile shifts to the right for  $\alpha = 0.5$  and to the left for  $\alpha = 1.5$ . Notice that the maximum of the PDF decreases slightly as  $\beta$  is raised from 0 in both cases.

Figure 6 shows the dependence of the probability density  $p$  at time  $t = 1$  on the intensity

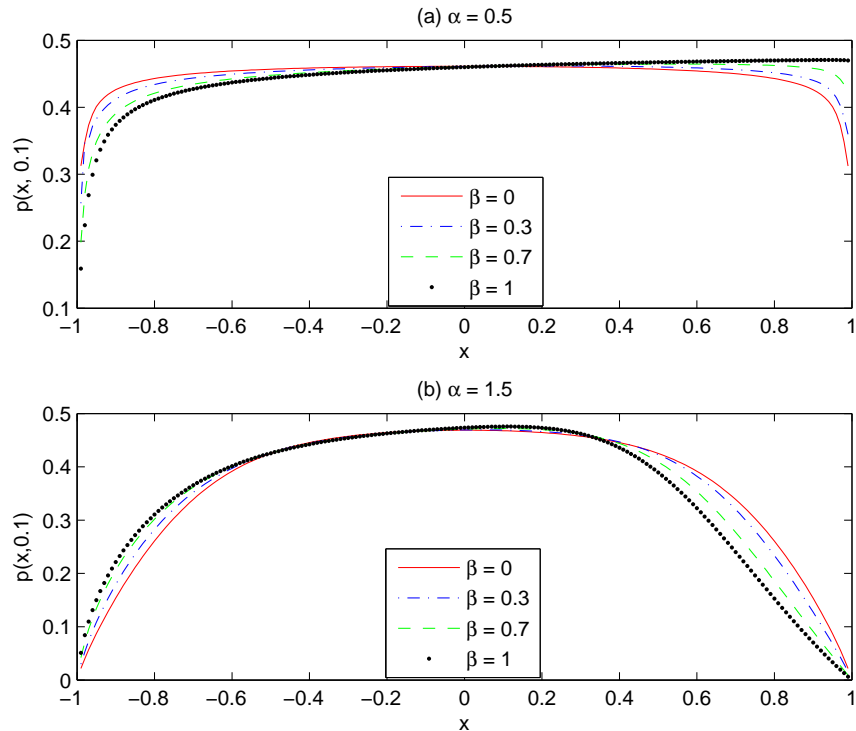


Figure 4: The effect of the skewness parameter  $\beta$ . (a) The PDFs at time  $t = 0.1$  are plotted for different values of  $\beta = 0, 0.3, 0.7, 1$  with  $\alpha = 0.5, f \equiv 0, \sigma = 0, \varepsilon = 1, D = (-1, 1)$  and the initial condition  $p(x, 0) = 0.5I_{\{|x| < 1\}}$ . (b) The same as (a) except  $\alpha = 1.5$ .

of Gaussian noise  $\sigma$ , where the initial profile is the Gaussian  $p(x, 0) = \sqrt{\frac{40}{\pi}}e^{-40x^2}$  and the other parameters are fixed at  $f \equiv 0, \beta = 0.5, \varepsilon = 1$  and  $D = (-1, 1)$ . Clearly, as one increases the amount of Gaussian noise  $\sigma$ , the process is less likely to stay in the domain  $D$  and the values of the PDFs become smaller. Besides, the profiles of the PDFs at  $t = 1$  are all concave downward and are smooth at the boundaries of the domain  $x = \pm 1$  for  $\sigma > 0$ . The graphs of the PDFs become more symmetric with respect to the center of the domain when there are more Gaussian noises or  $\sigma$  increases.

Keeping other parameters and the conditions as in Fig. 6, we examine the effect of the magnitude of non-Gaussian ( $\varepsilon$ ) noises in Fig. 7 using different values of  $\varepsilon = 0.1, 0.3, 0.7$  and 1. The numerical results show that, for  $\alpha = 0.5$ , the graphs of  $p$  develop a jump at the right boundary of  $D$  and become more skew to the right as  $\varepsilon$  is increased; for  $\alpha = 1.5$ , the PDFs become more skew to the left when the non-Gaussian noise level is raised.

Figure 8 shows that the variety of the densities at time  $t = 0.2$  for different domains  $D = (-1, 1), (-2, 2), (-4, 4)$  and different  $\alpha = 0.5, 1.5$  starting with the same Gaussian-type initial condition. The auxiliary condition is the absorbing condition and  $\beta = 0.5, \varepsilon = 1, \sigma = 0$  without the drift. From Fig. 8(a) corresponding to  $\alpha = 0.5$ , we find that the densities for the differently sized domains are almost identical on the interval  $(-1, 1)$ . It can be explained by realizing that most of the movement of the process governed by the SDE (2.1) consists of large jumps for  $\alpha = 0.5$ . For  $\alpha = 1.5$  as shown in Fig. 8(b), the probability finding the process near the peak  $(-0.4, 0)$  is about the same for all three sizes of the domain  $D$  but the density for the smallest domain  $D = (-1, 1)$  quickly goes to zero at the boundary  $x = \pm 1$ . It is interesting to note that the PDFs for the two larger domains  $D = (-2, 2)$  and  $(-4, 4)$  are almost identical on the interval  $(-1, 1)$ .

Further, we investigate the effect of drift  $f$ . Figure 9 shows the changes of probability densities

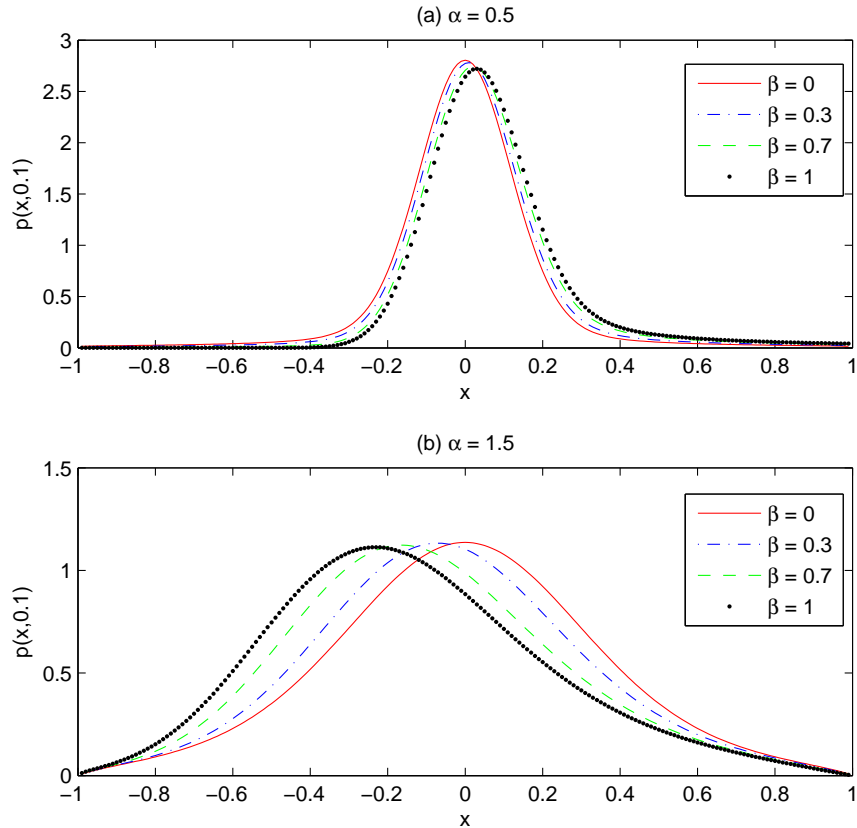


Figure 5: The effect of the skewness parameter  $\beta$  on the PDFs at time  $t = 0.1$  for  $f \equiv 0, \sigma = 0, \varepsilon = 1, D = (-1, 1)$  and the initial condition  $p(x, 0) = \sqrt{\frac{40}{\pi}} e^{-40x^2}$ . (a)  $\alpha = 0.5$ ; (b)  $\alpha = 1.5$ .

if we add the O-U potential  $f(x) = -0.6x$  for different  $\alpha = 0.5$ (Fig. 9(a)) and  $\alpha = 15$ (Fig. 9(b)) with  $\beta = 0.5, \sigma = 0, \varepsilon = 1, D = (-1, 1)$  starting with the initial profile of  $p(x, 0) = \sqrt{\frac{40}{\pi}} e^{-40x^2}$ . It can be seen that the densities become larger near the origin and more symmetric with respect to the center of the domain as expected.

Finally, we consider the effect of auxiliary conditions described in § 2.2. In Fig. 10, we plot the PDFs at the same time  $t = 0.2$  but with three different auxiliary conditions: the natural condition and the absorbing conditions for two domain sizes  $D = (-1, 1)$  and  $(-5, 5)$ . We keep the other parameters the same as those in Fig. 8. For both values of  $\alpha = 0.5$  and  $1.5$ , the PDF for the natural condition is slightly larger than the ones for the absorbing condition. For  $\alpha = 0.5$ , the PDFs for the three different auxiliary conditions are almost identical on the interval  $(-1, 1)$  except near the peak region. For  $\alpha = 1.5$ , the PDF for the absorbing condition with  $D = (-1, 1)$  drops to zero near the boundary of its domain  $x = \pm 1$  while the PDF for the absorbing condition with  $D = (-5, 5)$  is close to that of the natural condition on the interval  $(-1, 1)$ .

### 5.3 Most probable phase portrait (MPPP)

From the solutions to the Fokker-Planck equation (2.4), one can find the most probable orbits of stochastic dynamical systems (2.1) driven by asymmetric Lévy motion. MPPP, denoted by  $x_m(t)$ , is defined as the maximum of the PDF at time  $t$ , i.e.  $x_m(t) = \max_{x \in \mathbb{R}} p(x, t)$ , which gives the most probable orbit starting at  $x_0$  [10]. Figure 11 plots the MPPPs for  $\alpha = 0.5, \sigma = 0, \varepsilon = 1, D = (-1, 1), f(x) = -0.6x$  and different values of  $\beta = -0.5, 0, 0.5$ . To approximate the delta function

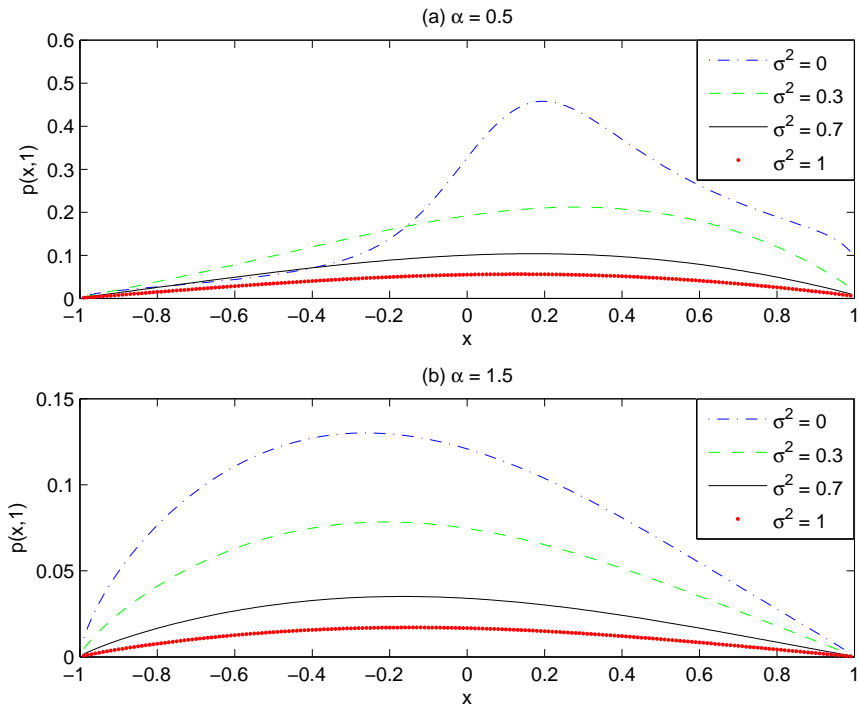


Figure 6: The effect of the intensity of Gaussian noise ( $\sigma^2 = 0, 0.3, 0.7, 1$ ) on the PDFs without drift ( $f \equiv 0$ ) at the fixed time  $t = 1$  with  $\beta = 0.5, \varepsilon = 1, D = (-1, 1)$  and the initial condition  $p(x, 0) = \sqrt{\frac{40}{\pi}}e^{-40x^2}$ . (a)  $\alpha = 0.5$ ; (b)  $\alpha = 1.5$ .

$\delta(x_0)$ , we choose the initial condition of Gaussian density function  $p(x, 0) = \sqrt{\frac{40}{\pi}}e^{-40(x-x_0)^2}$ . In absence of the noises, the system has the unique globally stable state at the origin  $x = 0$ . When we introduce the symmetric Lévy noises corresponding to  $\beta = 0$ , the process still goes to the origin independent of the initial starting point  $x_0$ . When the asymmetric Lévy noises are present ( $\beta = 0.5$ ), the MPPP approaches to a point different than the origin. It is interesting that MPPP converges to the same point for a fixed value of  $\beta$  regardless the initial condition.

## 6 Conclusion

Due to its wide range of applications of non-Gaussian Lévy noises in many disciplines, we study the Fokker-Planck equation with asymmetric  $\alpha$ -stable Lévy motion, which is a nonlocal (integro-differential) partial differential equation. The Fokker-Planck equation describes the time evolution of the probability density function. In this work, we show a symmetry property for solutions with respect to the sign of  $\beta$ , enabling us only need to consider the cases with  $\beta > 0$ . We have developed an accurate and fast numerical scheme for solving the FPEs for different auxiliary conditions (the absorbing condition and the natural condition). The numerical method is validated by comparing the numerical solution with a special exact solution and used to compute the solutions corresponding to different parameters in the system. We find that the PDFs are discontinuous at the right boundary when  $\alpha < 1$  and  $\beta > 0$  and the discontinuity becomes more evident when  $\beta$  increases; the discontinuity disappears for  $\alpha > 1$ . We have also considered the most probable phase portrait and find that the process approaches the same state when starting with different condition.



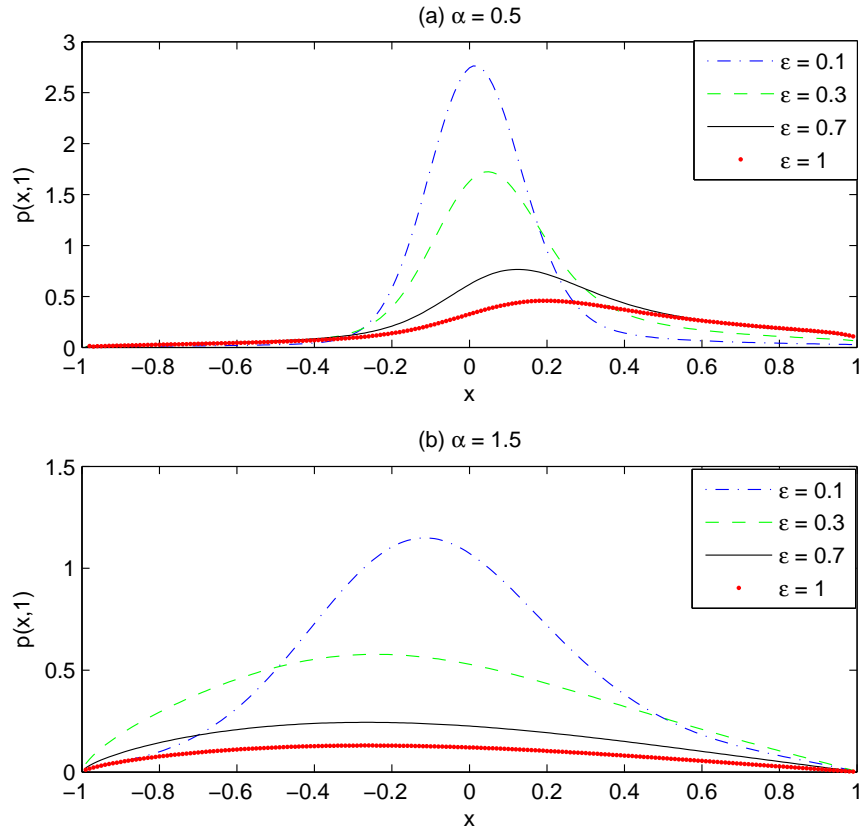


Figure 7: The effect of intensity of non-Gaussian noise ( $\varepsilon = 0.1, 0.3, 0.7, 1$ ) on the PDFs without the drift term ( $f \equiv 0$ ) at time  $t = 1$  with  $\sigma = 0, \beta = 0.5, D = (-1, 1)$  and the initial condition  $p(x, 0) = \sqrt{\frac{40}{\pi}} e^{-40x^2}$ . (a)  $\alpha = 0.5$ ; (b)  $\alpha = 1.5$ .

## 7 Acknowledgements

The research is partially supported by the grants China Scholarship Council #201306160071 (X.W.), NSF-DMS #1620449 (J.D. and X.L.), National Natural Science Foundation of China grants 11531006 and 11771449 (J.D.).

## References

- [1] G. Acosta and J. Borthagaray. A fractional Laplace equation: Regularity of solutions and finite element approximations. *SIAM J. Numer. Anal.*, 55(2):472–495, 2017.
- [2] G. Acosta, J. Borthagaray, O. Bruno, and M. Maas. Regularity theory and high order numerical methods for the (1D)-fractional Laplacian. *Math. Comput.*, In press, 2018.
- [3] D. Applebaum. *Lévy Processes and Stochastic Calculus*. Cambridge University Press, Cambridge, U.K., 2nd edition, 2009.
- [4] A. Cartea and D. del Castillo-Negrete. Fractional diffusion models of option prices in markets with jumps. *Phys. A, Stat. Mech. Appl.*, 374(2):749–763, 2007.
- [5] Z. Chen, E. Hu, L. Xie, and X. Zhang. Heat kernels for non-symmetric diffusion operators with jumps. *J. Differ. Equations*, 263(10):6576–6634, 2017.

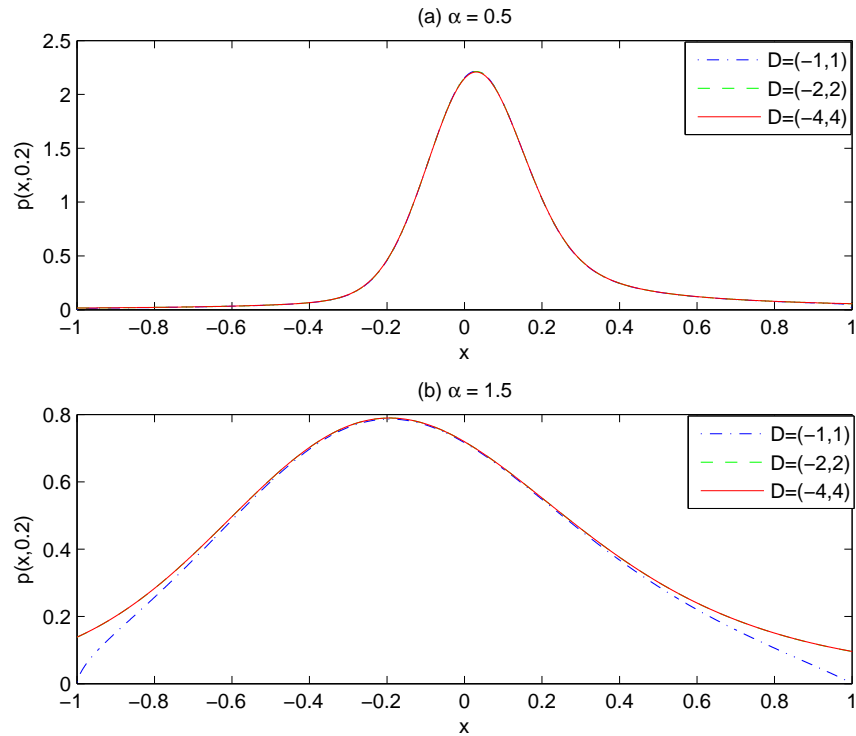


Figure 8: The effect of the domain size  $D(D = (-1, 1), (-2, 2), (-4, 4))$  for the absorbing condition with  $\beta = 0.5, \sigma = 0, \varepsilon = 1, f \equiv 0$ , at  $t = 0.2$ . The initial condition is the Gaussian density function  $p(x, 0) = \sqrt{\frac{40}{\pi}}e^{-40x^2}$ . (a)  $\alpha = 0.5$ ; (b)  $\alpha = 1.5$ .

- [6] Z. Chen and X. Zhang. Heat kernels and analyticity of non-symmetric jump diffusion semi-groups. *Probab. Theory Rel.*, 165(1):267–312, 2016.
- [7] M. Cozzi. Interior regularity of solutions of non-local equations in Sobolev and Nikol’skii spaces. *Ann. Mat. Pura. Appl.*, 196(2):555–578, 2017.
- [8] M. D’Elia and M. Gunzburger. The fractional Laplacian operator on bounded domains as a special case of the nonlocal diffusion operator. *Comput. Math. Appl.*, 66(7):1245–1260, 2013.
- [9] Q. Du, M. Gunzburger, R. B. Lehoucq, and K. Zhou. Analysis and approximation of nonlocal diffusion problems with volume constraints. *SIAM Rev.*, 54(4):667–696, 2012.
- [10] J. Duan. *An Introduction to Stochastic Dynamics*. Cambridge University Press, 2015.
- [11] T. Gao, J. Duan, X. Li, and R. Song. Mean exit time and escape probability for dynamical systems driven by Lévy noise. *SIAM J. Sci. Comput.*, 36(3):A887–A906, 2014.
- [12] C. W. Gardiner. *Handbook of Stochastic Methods*. Springer, 3rd Ed., 2004.
- [13] G. H. Golub and C. F. Van Loan. *Matrix computations*. JHU Press, 4th Ed., 2012.
- [14] G. Grubb. Fractional Laplacians on domains, a development of Hormander’s theory of u-transmission pseudodifferential operators. *Adv. Math.*, 268:478–528, 2015.
- [15] M. Hao, J. Duan, R. Song, and W. Xu. Asymmetric non-Gaussian effects in a tumor growth model with immunization. *Appl. Math. Model.*, 38:4428–4444, 2014.

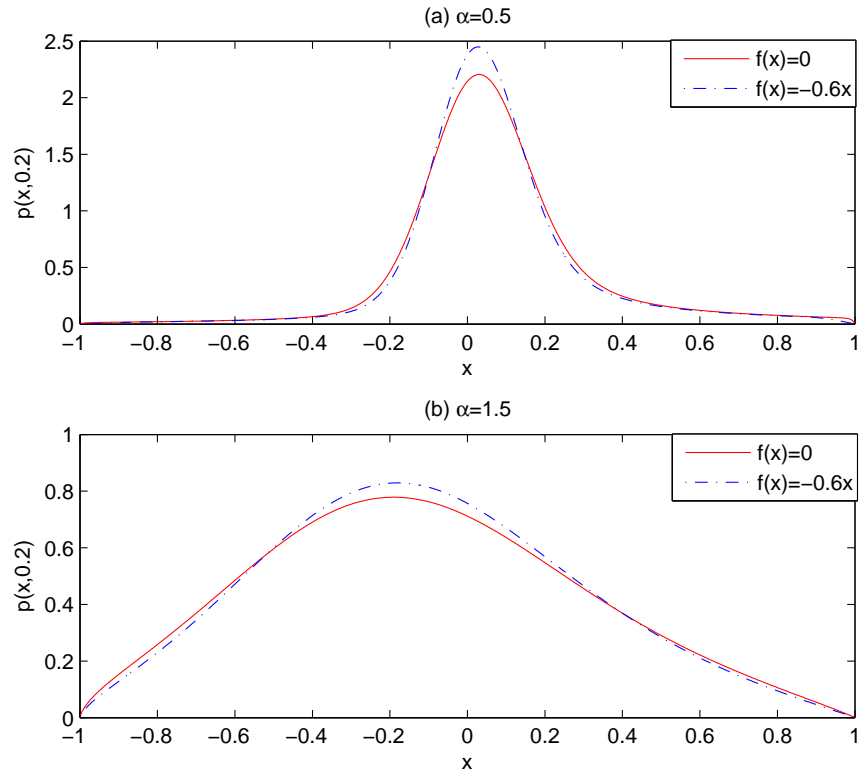


Figure 9: The effect of the drift  $f(f(x) = 0$  or  $-0.6x$ ) on the PDFs at time  $t = 0.2$  with  $\beta = 0.5, \sigma = 0, \varepsilon = 1, D = (-1, 1)$  and the initial condition  $p(x, 0) = \sqrt{\frac{40}{\pi}} e^{-40x^2}$  for  $\alpha = 0.5$ (a),  $\alpha = 1.5$ (b).

- [16] C. Hein, P. Imkeller, and I. Pavlyukevich. Limit theorems for p-variations of solutions of SDEs driven by additive stable Lévy noise and model selection for paleo-climatic data. *Interdiscip. Math. Sci.*, 8:137–150, 2009.
- [17] Q. Huang, J. Duan, and J. Wu. Maximum principles for nonlocal parabolic waldenfels operators. *arXiv:1607.02836*, 2016.
- [18] Y. Huang and A. Oberman. Numerical methods for the fractional Laplacian: A finite difference-quadrature approach. *SIAM J. Numer. Anal.*, 52(6):3056–3084, 2014.
- [19] N. Humphries *et al.* Environmental context explains Lévy and Brownian movement patterns of marine predators. *Nat. Lett.*, pages 1066–1069, 2010.
- [20] T. Koren, A. Chechkin, and J. Klafter. On the first passage time and leapover properties of Lévy mmotion. *Physica A*, 379:10–22, 2007.
- [21] M. Kwasnicki. Ten equivalent definitions of the fractional Laplace operator. *Fract. Calc. Appl. Anal.*, 20(1):7–51, 2017.
- [22] F. Liu, V. Anh, and I. Turner. Numerical solution of the space fractional Fokker-Planck equation. *J. Comput. Appl. Math.*, 166:209–219, 2004.
- [23] Z. Mao and J. Shen. Efficient Spectral-Galerkin method for fractional partial differential equations with variable coefficients. *J. Comput. Phys.*, 307:243–261, 2016.

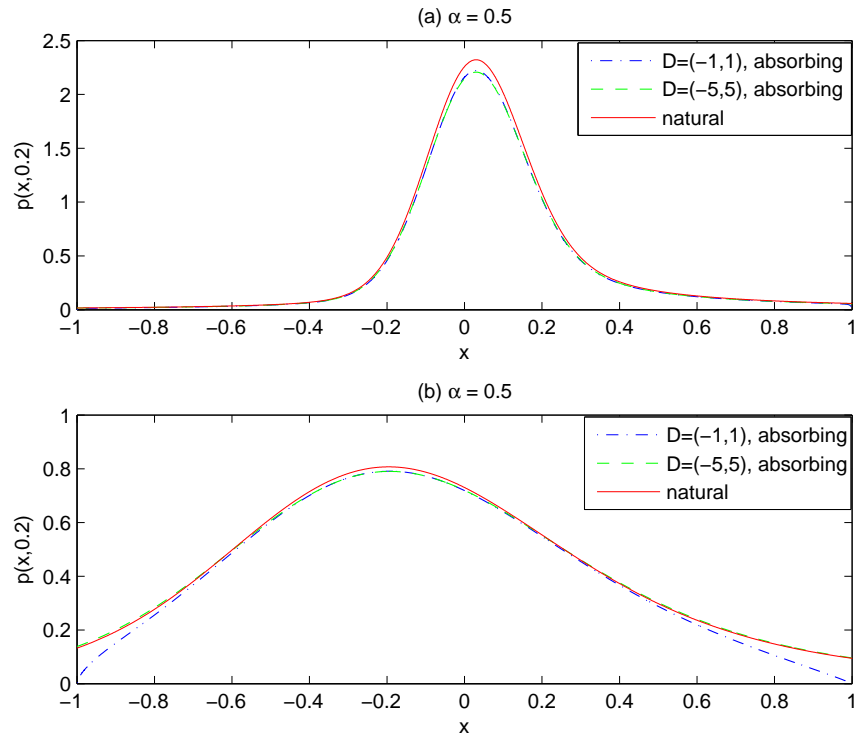


Figure 10: Comparison of the PDFs at time  $t = 0.2$  between the natural condition and the absorbing condition for the domains  $D = (-1, 1)$  and  $(-5, 5)$  with  $\beta = 0.5, \sigma = 0, \varepsilon = 1, f \equiv 0$  and the initial condition of  $p(x, 0) = \sqrt{\frac{40}{\pi}}e^{-40x^2}$ . (a)  $\alpha = 0.5$ ; (b)  $\alpha = 1.5$ .

- [24] Z. Mao and J. Shen. Hermite spectral methods for fractional PDEs in unbounded domains. *SIAM J. Sci. Comput.*, 39(5):A1928–A1950, 2017.
- [25] M. Riabiz and S. Godsill. Approximate simulation of linear continuous time models driven by asymmetric stable Lévy processes. *IEEE International Conference on Acoustics, Speech and Signal Processing (ICASSP), New Orleans, LA, 2017*, pages 4676–4680, 2017.
- [26] H. Risken. *The Fokker-Planck Equation Methods of Solution and Applications*. Springer-Verlag Berlin Heidelberg, 2nd edition, 1996.
- [27] X. Ros-Oton and J. Serra. The Dirichlet problem for the fractional Laplacian: Regularity up to the boundary. *J. Math. Pure. Appl.*, 101(3):275–302, 2014.
- [28] G. Samorodnitsky and M. S. Taqqu. *Stable Non-Gaussian Random Process*. Chapman & Hall/CRC, 1994.
- [29] K. I. Sato. *Lévy Processes and Infinitely Divisible Distributions*. Cambridge University Press, 1999.
- [30] D. Schertzer, M. Larcheveque, V. V. Duan, J. and Yanovsky, and S. Lovejoy. Fractional Fokker-Planck equation for nonlinear stochastic differential equations driven by non-Gaussian Lévy stable noises. *J. Math. Phys.*, 42(1):200–212, 2001.
- [31] A. Sidi and M. Israeli. Quadrature methods for periodic singular and weakly singular fredholm integral equataions. *J. Sci. Comput.*, 3(2):201–231, 1998.

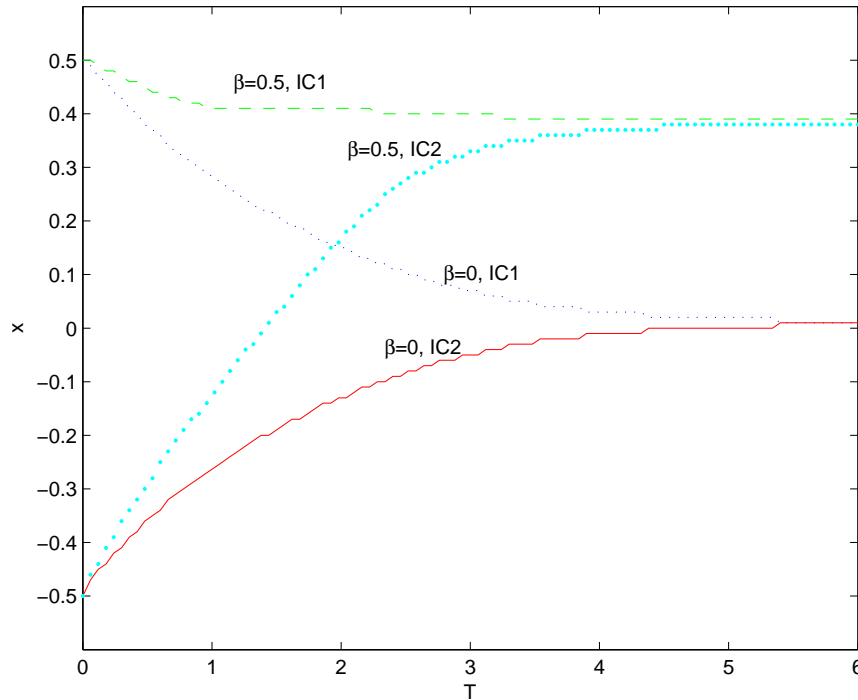


Figure 11: The MPPP for different  $\beta = 0, 0.5$  with the drift term  $f(x) = -0.6x$  and  $\alpha = 0.5, d = 0, \varepsilon = 1, D = (-1, 1)$ . The initial condition 1(IC1) and 2(IC2) correspond to the Gaussian density functions  $p(x, 0) = \sqrt{\frac{40}{\pi}}e^{-40(x-0.5)^2}$  and  $p(x, 0) = \sqrt{\frac{40}{\pi}}e^{-40(x+0.5)^2}$ , respectively.

- [32] T. Srokowski. Asymmetric Lévy flights in nonhomogeneous environments. *J. Stat. Mech.-Theory E.*, 2014(5):P05024, 2014.
- [33] X. Tian and Q. Du. Nonconforming discontinuous Galerkin methods for nonlocal variational problems. *SIAM J. Numer. Anal.*, 53(2):762–781, 2015.
- [34] M. Wang and J. Duan. Existence and regularity of a linear nonlocal Fokker-Planck equation with growing drift. *J. Math. Anal. Appl.*, 449(1):228–243, 2017.
- [35] X. Wang, J. Duan, X. Li, and Y. Luan. Numerical methods for the mean exit time and escape probability of two-dimensional stochastic dynamical systems with non-Gaussian noises. *Appl. Math. Comput.*, 258:282–295, 2015.
- [36] X. Wang, J. Duan, X. Li, and R. Song. Numerical algorithms for mean exit time and escape probability of stochastic systems with asymmetric Lévy motion. *arXiv:1702.00600*, 2017.
- [37] J. Wei and R. Tian. Well-posedness for the fractional Fokker-Planck equations. *J. Math. Phys.*, 56(3):1–12, 2015.
- [38] Y. Xu, J. Feng, J. Li, and H. Zhang. Lévy noise induced switch in the gene transcriptional regulatory system. *Chaos*, 23(1):013110, 2013.
- [39] L. Zeng and B. Xu. Effects of asymmetric Lévy noise in parameter-induced aperiodic stochastic resonance. *Physica A*, 389:5128–5136, 2010.

